

Electronic Supplementary Information file for article:

XANES study of Vanadium and Nitrogen dopants in photocatalytic TiO₂ thin films

by

Zakaria El Koura, Giacomo Rossi, Marco Calizzi, Lucia Amidani, Luca Pasquini, Antonio Miotello, Federico Boscherini

EXPERIMENTAL AND THEORETICAL METHODS

Sample preparation and characterization

Before each deposition, a base pressure of about 10^{-7} mbar was achieved in the deposition chamber of the RF-sputtering and the target was pre-sputtered for 20 minutes to remove all possible contaminants from the surface. The target-substrate distance was kept constant at 6.0 cm, and the substrate holder was kept oscillating in the plasma to improve the homogeneity of the films.

X-ray absorption spectroscopy measurements and data analysis

In the measurements at the BM23 beamline, the incident energy was selected using a double bounce flat crystal Si (111) monochromator. The Vortex Si drift diode detector was placed in the horizontal plane at right angles to the impinging beam.

The following reference compounds (Ti and V oxides) were measured in transmission mode using finely ground powders dispersed in polyethylene:

- TiO₂ anatase, Alfa Aesar, 99.6% (code: 36199)
- TiO₂ rutile, Alfa Aesar, 99.99% (code: 14631)
- V₂O₃, Sigma-Aldrich, 99.99% (code:463744)
- VO₂, Alfa Aesar, 99% (code: 22957)
- V₂O₅, Sigma-Aldrich, 99.6 % (code: 221899)

For High Energy Resolution Fluorescence Detected (HERFD) XANES measurements at ID26 beamline, the V K α_1 fluorescence (4952.2 eV) from the samples was selected and focused on an avalanche photodiode (APD) by five spherically bent ($R = 1$ m) Ge crystals in (331) reflection. The incident energy was selected by the Si (311) reflection of a double crystal monochromator, and higher harmonics were rejected by three Si mirrors under total external reflection.

For the processing of EXAFS spectra using Athena [1], the pre-edge region was fitted with a linear function while the post – edge region was fitted with a spline to simulate the atomic cross section. As a first approximation the energy origin for the energy – to – wavenumber conversion (E_0) was chosen as the maximum of the first derivative of the absorption spectrum.

A state of the art EXAFS analysis at the Ti K-edge including multiple scattering (MS) contributions was carried out on highly crystalline thin films and on reference anatase. Based on the crystallographic structure, the single (SS) and MS contributions to the fine structure oscillations were calculated using the FEFF code [2]. Using ARTEMIS [1] the spectra were fitted excluding those paths which gave a negligible contribution. Fitting parameters were an energy origin shift, a single isotropic distance variation parameter and individual Debye – Waller (DW) factors for each path. Spectra were fitted in the range $k = 4.0 - 11 \text{ \AA}^{-1}$ and $R = 1.1 - 3.9 \text{ \AA}$. We found that the following paths were necessary for a meaningful fit: SS contributions related to the six O nearest neighbors (1st and 2nd shell, fitted as a single component in view of the small distance splitting) and the four Ti ions in the 3rd and 4th coordination shell and a single three - legged MS contribution involving the O nearest neighbors and the Ti in the 4th coordination shell. The path degeneracies were kept fixed at the values of the crystals since, due to the well known high correlation with Debye – Waller factors, it was impossible to determine them with a reasonable uncertainty.

Calculation of relaxed doped structures

Models for the local structure of doped TiO₂ were obtained modifying rutile and anatase clusters. Undoped crystal structures were obtained from literature [3]. For the self-consistent field calculation (SCF) we used Vanderbilt ultra-soft pseudopotentials [4] with the Perdew-Burke-Ernzerhof exchange correlation functional [5] selected from the Quantum Espresso repository [6] (files Ti.pbe-sp-van_ak.UPF, V.pbe-sp-van.UPF, N.pbe-van_ak.UPF and O.pbe-van_ak.UPF). The cutoff energy for the wave functions of the plane wave algorithm was set to 30 Ry. The k space sampling was done using a 4 x 4 x 4 mesh while the structural optimization was performed using the BFGS algorithm [7,8] iterated until the total cluster force reached a value lower than $1 \cdot 10^{-3} \frac{\text{Ry}}{a_0}$. For one of the V-N-TiO₂ models (M4), however it was impossible for us to achieve a total cluster force lower than $1 \cdot 10^{-2} \frac{\text{Ry}}{a_0}$. This could be related to a higher instability of that configuration.

In Table S1 we list the vector basis of the relaxed super cell structures compared to those of pure anatase and rutile. The full atomic coordinate sets in Cartesian units are provided in a separate archive.

Supplementary Figures and Tables

Table S1: Crystallographic parameters of relaxed doped super-cells. The * indicates pure compounds obtained joining multiple anatase and rutile unit cells.

Model	a (Å)	b (Å)	c (Å)	α (°)	β (°)	γ (°)
Anatase *	7.585	7.585	19.313	90	90	90
Rutile *	9.187	9.187	8.874	90	90	90
V_{Ti}	7.585	7.585	19.313	90.00	90.00	90.00
V_i	7.625	7.625	19.226	90.02	90.00	90.00
Model 1	7.606	7.575	19.281	90.00	89.99	90.00
Model 2	7.594	7.572	19.307	90.00	90.00	90.00
Model 3	7.563	7.575	19.439	89.86	90.04	90.00
Model 4	7.584	7.578	19.387	90.04	90.25	89.99
Model 5	7.597	7.592	19.372	90.00	90.00	90.00
Model 6	7.457	7.581	20.152	89.61	90.21	90.15
Model 7	9.279	9.279	8.904	89.99	89.99	90.42

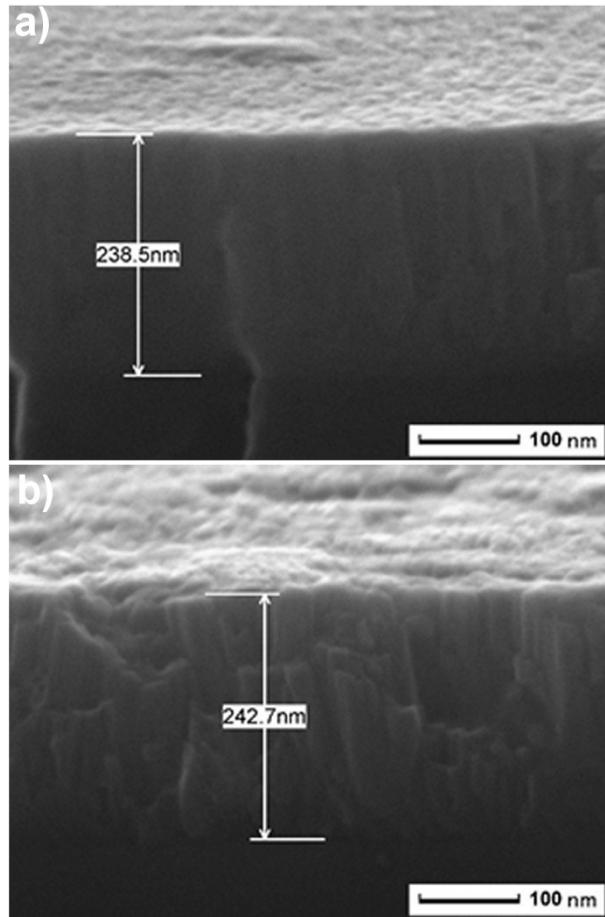


Figure S1: Cross sectional SEM image of amorphous (a) and crystalline (b) V-TiO₂ films.

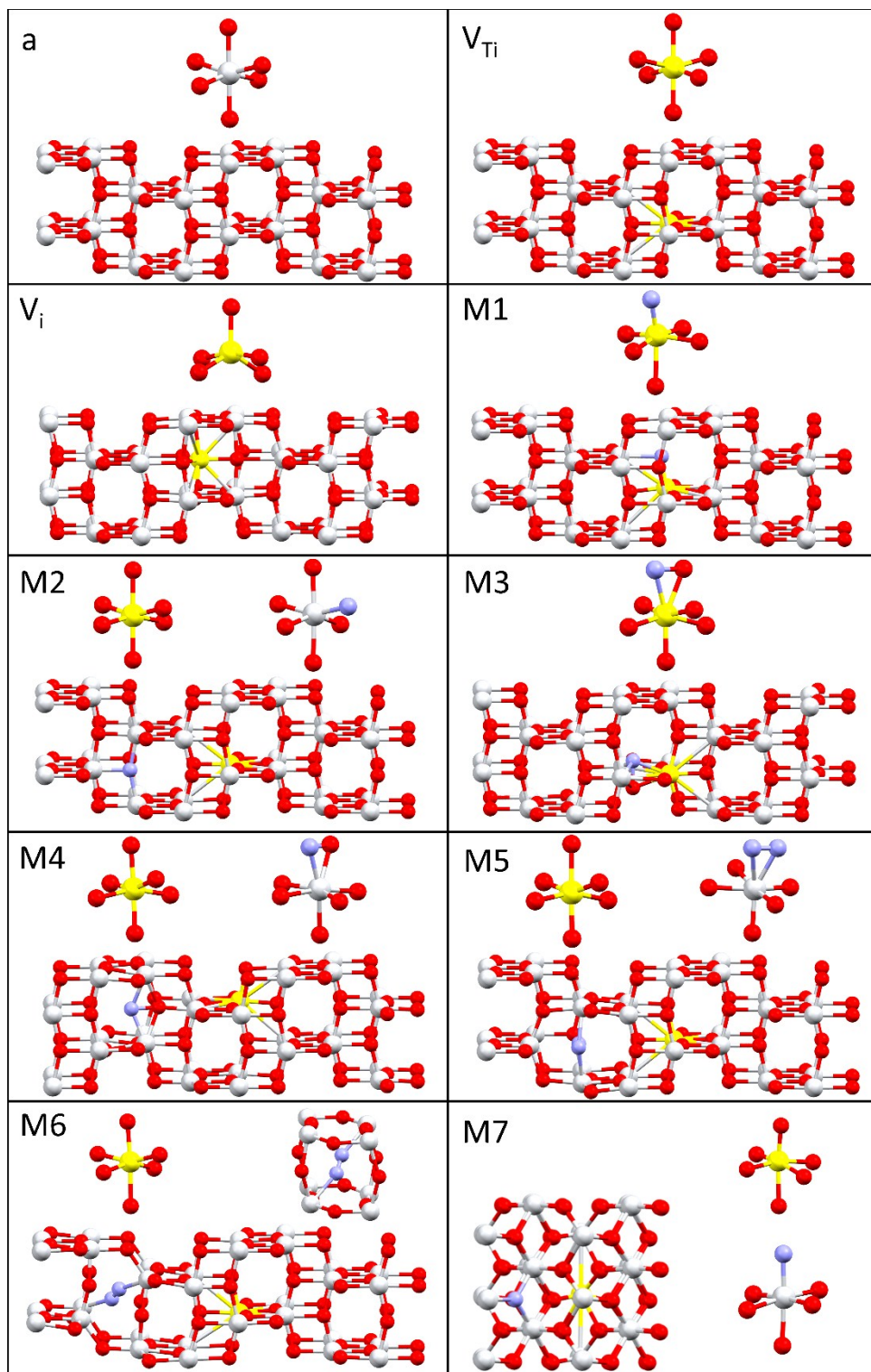


Figure S2: Relaxed structures for V-doped and V-N-codoped TiO_2 . Ti in grey, V in yellow, O in red and N in blue. a: anatase TiO_2 ; V_{Ti} : substitutional V in anatase; V_i : interstitial V in anatase; M1-M6: V-N-codoped anatase; M7: V-N-codoped rutile.

Table S2: Description of the starting and relaxed dopant configuration for all calculated models of V and N dopants in TiO₂. Only model M7 refers to rutile, while the other models are for anatase. The images of the corresponding relaxed structures are displayed in Figure S2.

Model Label	Starting configuration	Relaxed configuration
V _{Ti}	V substitutes Ti.	V does not produce evident structural distortions. The V-centered octahedron slightly shrinks
V _i	V is placed in an interstitial site	V reaches a stable position at the center of a rhomboidal-based pyramid (Fig. S2-c)
M1	V substitutes Ti and N replaces one neighboring O	The octahedron with the two dopants is heavily distorted
M2	V and N substitute Ti and O in different octahedra	The dopant-containing octahedra are quite similar to anatase
M3	V substitutes Ti. N is in an interstitial site near the V octahedron	N is attracted by the V octahedron and shares a corner with one O
M4	V substitutes Ti. N is in an interstitial site far from the V octahedron	N is attracted by a Ti-centered octahedron and shares one corner with an O. Quite unstable and difficult to relax
M5	V substitutes Ti. Far from the V dopant, a N ₂ dimer substitutes one O in a Ti octahedron	The octahedron containing the two N atoms is slightly distorted compared to the anatase ones
M6	V substitutes Ti. A N ₂ dimer is placed in an interstitial site far from V.	The N ₂ dimer is not split by the crystal field, while the surrounding crystal structure is clearly perturbed
M7	V and N substitute Ti and O in two distant octahedra of the rutile structure.	The dopant-containing octahedra are quite similar to rutile

Table S3: Numerical results of quantitative EXAFS analysis carried out on reference anatase and V-TiO₂ crystalline thin films with different V content (2.4 and 4.5 at.% V). Numbers in brackets indicate uncertainties in best estimates.

Path	legs	N	Anatase		2.4 at.% V		4.5 at.% V	
			R (Å)	σ^2 (Å ²)	R (Å)	σ^2 (Å ²)	R (Å)	σ^2 (Å ²)
O (1 st /2 nd)	2	6	1.9565 (99)	0.0055 (12)	1.949 (11)	0.0050 (14)	1.948 (11)	0.0048 (14)
Ti (3 rd)	2	4	3.055 (15)	0.0058 (12)	3.058 (15)	0.0055 (15)	3.050 (15)	0.0051 (15)
Ti (4 th)	2	4	3.804 (19)	0.0040 (31)	3.690 (26)	0.0003 (26)	3.690 (25)	0.0007 (27)
O (1 st /2 nd) Ti (4 th)	3	8	3.849 (20)	0.0075 (17)	3.797 (23)	0.0012 (23)	3.800 (23)	0.0017 (23)

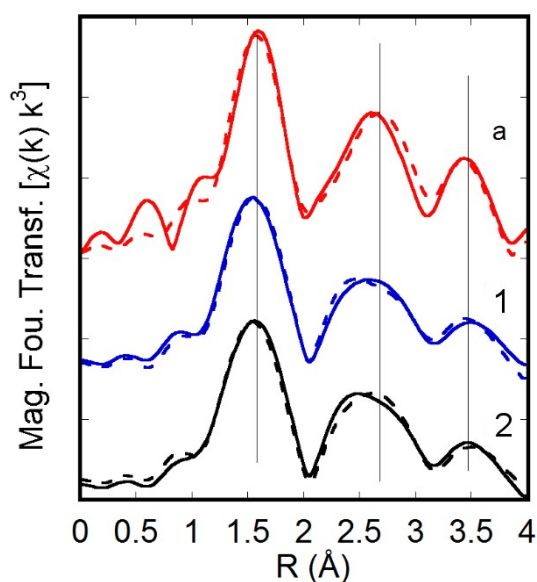


Figure S3: Magnitude of the Fourier Transform of Ti K-edge EXAFS spectra of the V-TiO₂ crystalline thin films with different V content (1= 2.4 at.% V; 2= 4.5 at.% V), compared to reference anatase (a). The Fourier transform was performed in the range $k = 4.0 - 11 \text{ \AA}^{-1}$ with a k^3 weight. Dashed lines represent high quality fits.

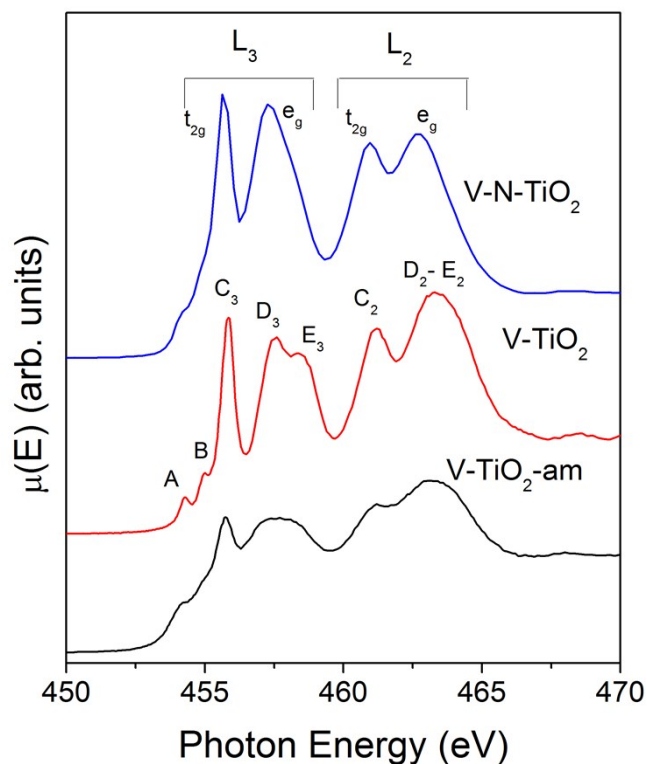


Figure S4: Ti L_{2,3} – edge XANES spectra. The features related to the L₃ and L₂ edges and to transitions to t_{2g} and e_g orbitals can be interpreted by crystal field multiplet calculations taking account the effects of local distortions, which eliminate the degeneracy of the t_{2g} and e_g states. Here the individual peaks are labelled according to previous papers [9].

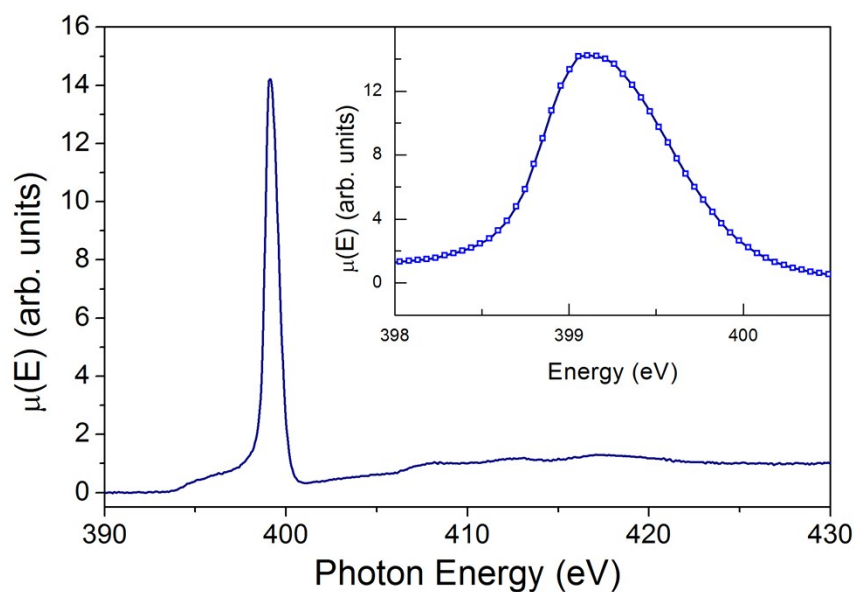


Figure S5: N K XANES measured on V-N-TiO₂ film. The inset displays a zoomed view of the intense white line, which demonstrate the absence of the vibrational structure characteristic of gaseous N₂.

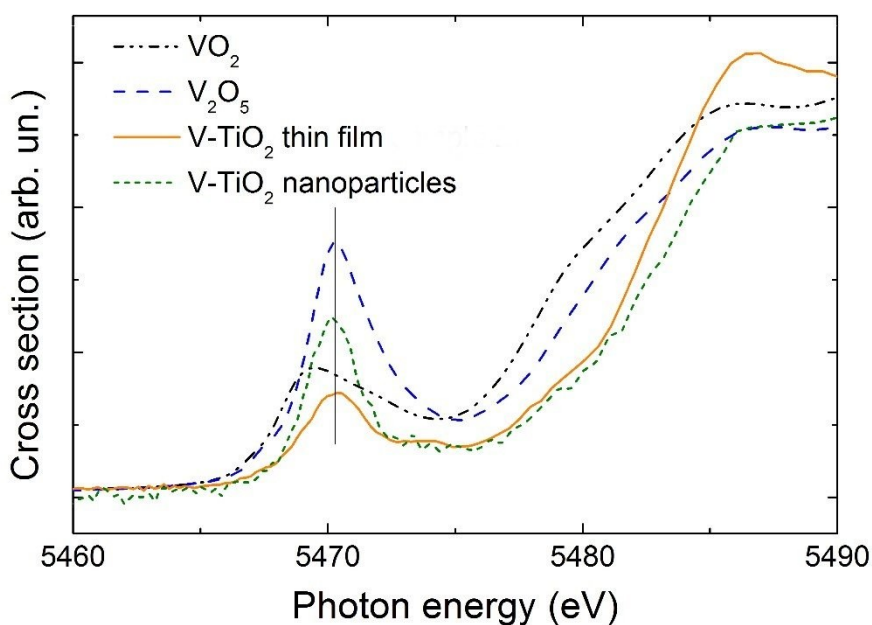


Figure S6: Detail of the pre-edge peak at the V K-edge XANES for reference V oxides, V-TiO₂ thin film (4.5 at.% V), and V-doped TiO₂ nanoparticles (mainly anatase, 3.5 at.% V) prepared by gas-phase condensation [10].

References

- [1] B. Ravel and M. Newville, *J. Synchrotron Radiat.* **12**, 537 (2005).
- [2] S. I. Zabinsky, J. J. Rehr, A. Ankudinov, R. C. Albers, and M. J. Eller, *Phys. Rev. B* **52**, 2995 (1995).
- [3] R. W. G. Wyckoff, *Crystal Structures*. (1960).
- [4] D. Vanderbilt, *Phys. Rev. B* **41**, 7892 (1990).
- [5] J. P. Perdew, K. Burke, and M. Ernzerhof, *Phys. Rev. Lett.* **77**, 3865 (1996).
- [6] <http://www.quantum-espresso.org/pseudopotentials/> [June 2017].
- [7] M. Avriel, *Nonlinear Programming: Analysis and Methods*, Dover Publishing (2003).
- [8] C. G. Broyden, *IMA J. Appl. Math.* **6**, 76 (1970).
- [9] S. O. Kucheyev, T. van Buuren, T. F. Baumann, J. H. Satcher, T. M. Willey, R. W. Meulenberg, T. E. Felter, J. F. Poco, S. A. Gammon, and L. J. Terminello, *Phys. Rev. B* **69**, 245102 (2004).
- [10] G. Rossi, M. Calizzi, V. Di Cintio, S. Magkos, L. Amidani, L. Pasquini, and F. Boscherini, *J. Phys. Chem. C* **120**, 7457 (2016).